Probing the pH Modulation of a Hyper-Phosphorylated Model of Alpha-B Crystallin

Kashmeera Devi Baboolall

Abstract

Acknowledgement

Contents

List of Figures

Chapter 1

Introduction

A widely-believed paradigm in biochemistry describes how amino acid sequence determines protein structure, which in turn influences protein function. While broadly accurate, this model fails to account for the role of environmental factors, post-translational modifications and neighbouring biomolecules on the final organization of proteins.

The rationale explained by the sequence-structure-function chain is inadequate when trying to answer questions about α-crystallin function and dynamics. α-crystallin functions as a chaperone that maintains the correct structures of intracellular proteins. α-crystallin achieves its chaperone function by forming oligomers whose sizes depend on environmental conditions and the size of α-crystallin's target biomolecule. Post-translational factors such as phosphorylation and succinylation also influence the size of oligomers formed by α-crystallin. α-crystallin thus illustrates how protein structure can be regulated by other factors.

Our work explores how post-translational phosphorylation modulates the oligomer size and chaperone function of α-Crystallin. We probe the dynamics our system using smFRET and FCCS. Light scattering experiments help us resolve the chaperone efficiences of the α-Crystallin variants under study.

This chapter provides a background on α-crystallin and its phosphorylation. Ideas such as sub-unit exchange and oligomerization are also explained to better appreciate the chaperoning mechanism of α-crystallin. Our research questions are described in greater detail at the end of this chapter.

The remaining chapters shed light on our experimental methods, the results obtained and an interpretation of the data. We also provide some insight for future steps in the project.

1.1 Alpha-B Crystallin

The maintenance of steady and well-balanced intracellular and physiological environments is conducive to and essential for the good health of organisms. Homeostasis and proteostasis can be viewed as homologous biological processes that help preserve an organism's health. While homeostasis is the maintenance of physiological equilibrium in living organisms, proteostasis refers to the intra-cellular regulation of proteins.

The correct folding of proteins is essential for proper cellular functioning and for the offset of diseases. A protein initially adopts its three-dimensional conformation when the Gibb's energy of its polypeptide chain drops to an absolute minimum in a thermodynamic funnel. Since most proteins require some degree of conformational freedom to carry out their functions, their native state thermodynamic stability is only marginal [98]. Post-translational modifications (truncation, methylation, deamidation, etc) and changes in cellular environments can compromise protein stability [131]. Unstable proteins often partially unfold or misfold, exposing hydrophobic sites on their polypeptide chains which then agglomerate. Protein aggregation results when such aggregates are not eliminated. Protein aggregates are cytotoxic and contribute to diseases and pathological conditions such as Alzheimer's disease, Parkinson's disease, Type 2 diabetes and Huntington's disease [57, 126, 1].

The proteostasis network is made up of chaperones and degradative factors that generate, maintain and eliminate proteins from the cell [19]. Molecular chaperones are proteins that interact with, stablize, or help another protein achieve its functionally viable structure, without being present in its final conformation [50]. Chaperones help in proteostasis by assisting protein folding, promoting the refolding of unfolded protein and limiting intracellular damage by "holding" potentially cytotoxic protein aggregates until they are safely degraded.

This section will describe α-Crystallin as a molecular chaperone and as a member of the small heat-shock proteins(SHSPs) class. The distinct structural features of α-Crystallin and their relevance to the protein's function will also be discussed. We will also highlight the influence of phosphorylation on α-Crystallin. Finally, we will present our research questions regarding α-Crystallin structure and function.

1.1.1 Small Heat-Shock Proteins(SHSPs) and Molecular Chaperone Functions

α-crystallin is a member of the small heat-shock protein(SHSPs) family which is itself a subset of the heat-shock protein(HSPs) superfamily. SHSPs are expressed in all kingdoms of life(Archaea, Bacteria and Eukarya) and viruses [46, 75, 113, 28]. SHSPs act as the first line of defence against factors threatening proteostasis and proteome stability [27]. Some characteristics of SHSPs include a conserved α-crystallin domain of about 90 residues, a small molecular mass of 12-43 kDa, formation of large oligomers, a dynamic quaternary structure, induction by stress conditions and chaperone activity to suppress protein aggregation [53]. 10 SHSPs(HSPB1-HSP10) are present in humans [9]. α-crystallin exists in two isoforms: αA-crystallin(HSPB4) and αB-crystallin(HSPB5). HSPB4 and HSPB5 share 57 sequence similarity and are expressed by the αA and αB genes respectively [101, 65]. Both αA-crystallin and αB-crystallin are highly expressed in the eye lens. While αA-crystallin is solely

localized in the eye lens, αB-crystallin is more ubiquitous and is present in many tissues throughout the body, especially in the heart muscles and the brain [61].

Structure of Small Heat-Shock Proteins

The α-crystallin domain(ACD) is the core fold that characterizes SHSPs. Though the individual amino acids making up the α-crystallin domain vary for different SHSPs, the immunoglobulin-like β sandwich of the α-crystallin domain is maintained throughout the SHSPs [10]. In metazoans, the α-crystallin domain is on average 91 amino acids long, making up 54% of SHSPs that span through an average of 167 amino acids. While the α-crystallin domain is highly conserved, the C-terminal domain and N-terminal domains of SHSPs are variable [72]. Studies have shown the importance of all three domains for sHSP function and oligomerization [91, 94, 87, 48].

αB-crystallin is 175 amino acids long, with an N-terminal domain of about 60 residues and a C-terminal domain of 25 residues [101]. The α-crystallin domain of αB-crystallin is made up of a β sandwich composed of two antiparallel β sheets made from nine β strands(Figure 1) [51]. A highly conserved IXI motif is also present on the usually variable C-terminal domain.

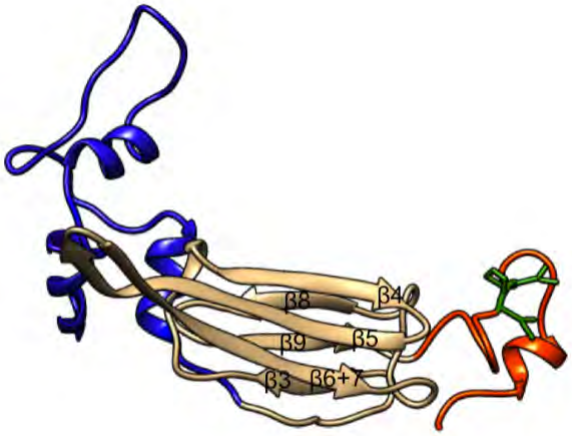

Figure 1.1: Hybrid of cryo-EM and NMR structure of αB-crystallin monomer(resolution : 9.5 Å). The N-terminal domain(blue) is least conserved. The C-terminal domain(red) is also variable but has a conserved IXI motif(green). The α-crystallin domain(cream) possesses a highly conserved β sandwich [19, 26]

Small Heat-Shock Proteins Function

It is thought that the variability in SHSPs sequences endows an organism's arsenal of SHSPs with the ability to detect a wide range of target proteins. In fact, studies of SHSPs systems present in yeast, *Escherichia coli* and *Synechocystis sp. PCC 6803* have shown that these SHSPs interact with a heterogeneous set of target proteins sharing no sequence, functional and structural similarities [56]. SHSPs maintain about one-third of cytosolic proteins treated under heat-shock conditions in a soluble state [53, 52]. The molecular chaperone function of SHSPs was first observed *in vitro* when α-crystallin was found to prevent the accumulation of aggregation-prone γ and β crystallins, two types of lens proteins present in the eyes [60]. This function was also confirmed *in vivo* when αA-crystllin knockout mice developed cytoplasmic inclusion bodies and cataract [22].

SHSPs bind to denatured proteins to prevent irreversible aggregation in an ATP-independent manner [71]. SHSPs function as 'holdases' and trap unfolding proteins to stablize them [51]. The substrate-sHSP interaction creates a reservoir of folding intermediates that help maintain the unfolded protein in a state conducive for refolding [43]. The extent to which chaperones imbibe unfolding proteins varies be-

tween different substrate-chaperone pairs and can reach up to stoichiometric quantities [128]. The aggregation suppression of ATP-dependent chaperones, often called 'foldases' , refold the proteins bound to the SHSPs (Figure 2). The HSP70/HSP40 system refolds substrates bound to SHSPs in mammalian and plant cells [83]. The reactivation mechanism depends on the ratio of sHSP to substrate. The chaperones must be large with respect to their targets to both bear enough hydrophobic portions to interact with target proteins and present enough hydrophilic portions to remain soluble [127]. The chaperone function of SHSPs is measured by the extent

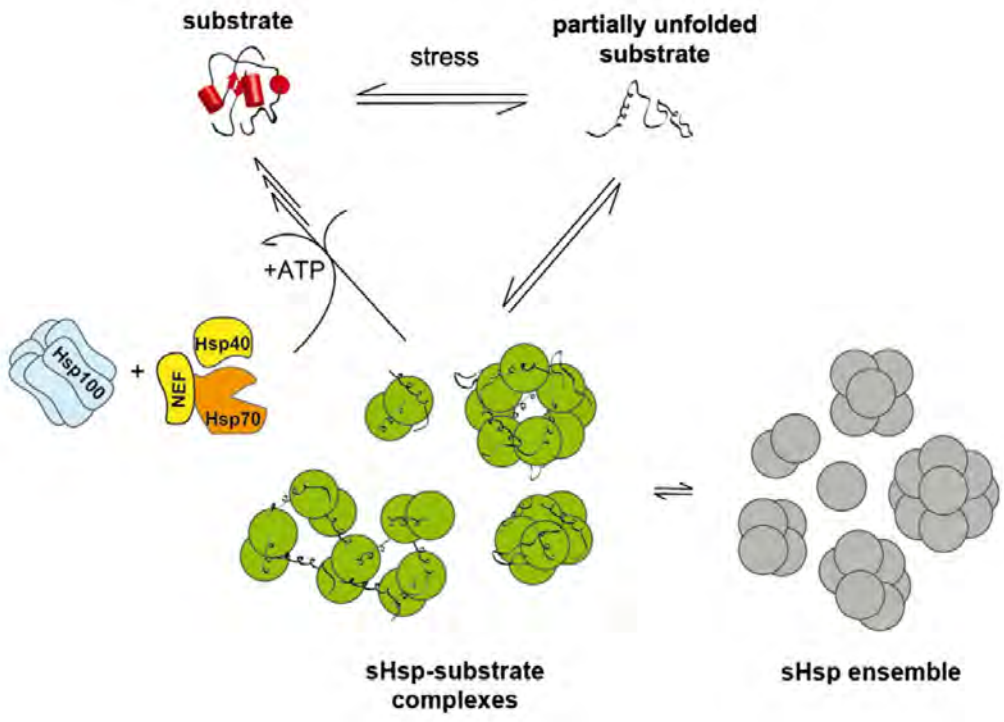

Figure 1.2: Schematic of the molecular chaperone function of SHSPs. Substrate proteins unfold and get destabilized under stress conditions. SHSPs bind to the unfolded proteins in an ATP-independent manner, holding them in a state fit for refolding. The HSP70/HSP40 chaperone system then refolds, in an ATP-dependent manner, the substrates on the sHSP-substrate. Image adapted from Ref. [51]

.

to which the kinetic competition between the binding of the substrate to the sHSP and the self-association of substrate is overcome so the substrate is rescued by the sHSP [92].

SHSPs can contribute to the proteostasis network via an alternate route: SHSPs

can direct substrates to the ubiquitin-proteosome pathway, one of the protein degradative systems of protein homeostasis [85, 45]. Unlike standard chaperones such as GroEL and DnaK, αB-crystallin does not usually bind to fully unfolded proteins [80]. αB-crystallin tends to interact with early non-native unfolding intermediates, helping them preserve their native secondary structure [34, 35]. This enables αB-crystallin maintain substrates in a state fit for refolding. The precise magnitude of unfolding needed for substrate recognition and rescue is ambiguous as it seems substrate-dependent [101].

Small Heat-Shock Proteins Regulation and Modulation

SHSPs expression and function need to be modulated due to their vital roles in the protein homeostasis pathway. While a deficiency in SHSPs can lead to the harmful agglomeration of denatured proteins in cells, an overactivity of SHSPs can sequester transient intermediates, pushing protein folding thermodynamics equilibrium away from the native state [92]. Heat shock and other stress conditions lead to the rapid induction of genes producing SHSPs [78]. While heat shock induces αB-crystallin expression, heat stress is not a necessary condition for the chaperone function of αB-crystallin which presents chaperone activity below heat shock temperatures [33, 47]. The concentration of SHSPs present in different cellular environmets changes as a response to cellular development, stress conditions such as hypoxia, oxidation and pathological status [129]. *In vitro* changes in pH environment also influence αB-crystallin chaperone function [107, 14, 86]. Studies have also highlighted the influence of bivalent metal ions (Zn^{2+}, Ca^{2+}, Mg^{2+}) binding on the chaperone activity of αB-crystallin [15, 29, 73]. SHSPs activity is also modulated by post-translational modifications [59]. Phosphorylation and succinylation, for instance, influence the activity of αB-crystalin [6, 97]. The effects of post-translational modifications on αB-crystallin will be further discussed in the next subsection.

The Numerous Functions of αB-Crystallin

As a member of the crystallin family, α-crystallin maintains the refractive properties and transparency of the eye lens. The eye lens is a biological optical instrument that focuses light from the cornea onto the retina without any spherical aberration for proper vision [80]. The gradual increase of the lens refractive index from 1.37 to 1.41 from the lens edge to its center helps correct for spherical aberrations [74]. The dense packing of crystallins creates the high refractive lens needed to focus light in the eyes [3]. αB-crystallin makes up 40% of the soluble proteins in lens fibre cells, reaching concentrations of about 430 mg ml^{-1} [17, 38]. It has been shown that beyond a protein concentration of 200 mg ml^{-1}, light scattering is greatly quenched [38] . The short range order of macromolecules induced by hard sphere interactions endows the lens with transparency at high protein concentrations [104]. Protein aggregates of the order of 50 MDa cause light scattering, rendering the lens turbid and eventually leading to cataract [12]. α-crystallin limits its self-aggregation to avoid the disruption of short-range interactions by forming a polydisperse distribution of oligomers that can dynamically sub-unit exchange (1.1.2). The cytoskeleton is an important structural component of lens cells. α-crystallin can also control the dynamic assembly of the lens cytoskeleton by regulating the cytoskeletal substrates fit for assembly [18]. α-crystallin can inhibit gel formation by limiting interactions between intermediate filaments [99]. Apart from its structural role, αB-crystallin also performs its molecular chaperone function in the lens. The 'holdase' function of αB-crystallin is crucial for cataract prevention. The lens is made up of fibre cells that lack cytoplasmic organelles that would otherwise contribute to light scattering [11]. Protein turnover is nonexistent in the eye lens due to the absence of cellular machinery required for protein degradation and replacement. It is therefore essential for lenticular proteins to remain stable throughout a person's lifetime. As aforementioned, unstable proteins can agglomerate to form longer range structures of cataractogenic potential. Though α-crystallin binds to unstable, partially

folded lenticular proteins, it cannot transfer these substrates further in the protein homeostasis pathway for either refolding or degradation. α-crystallin thus acts as a molecular sponge until it is saturated with substrates. At such high ratios of bound substrate to chaperone, α-crystallin has a great risk of self-aggregating, forming larger structures capable of scattering light in the lens. Crystallins also undergo age-related modifications such as oxidation, glycation, deamidation, truncation and methylation [122]. Such modifications deeply influence α-crystallin. Deamidation of the N_{146} residue on αB-crystallin compromises its structural integrity and limits its chaperone efficiency [90]. *In vitro* glycation of αB-crystallin adversely affects its 'holdase' function [40]. As the levels of antioxidants in the lens decline with age, α-crystallin becomes more vulnerable to oxidative damage [79]. Oxidation alters the secondary structure of α-crystallin, changing its oligomeric state and inhibits its chaperoning ability, thus leading to cataract [108]. α-crystallin is therefore a crucial lens protein that serves both structural and proteostatic functions that help limit the onset of cataracts.

αB-crystallin, Hsp27 and Hsp20 are the most common SHSPs found in cardiac cells. αB-crystallin is the most abundant of these three SHSPs, with expression levels varying between 0.1% and 2% of the soluble protein content [30]. Titin is a biological spring made up of different folded protein domains interconnected by peptide strands, that maintains elasticity of cardiac muscles. αB-crystallin stabilizes the domains in the N2B element of titin, thus increasinsg the stretching forces needed to unfold the folded protein domains [25]. While the abundance of mitochondria in cardiac cells ensures that their energetic and metabolic demands are maintained, the presence of mitochondria also puts cardiac cells at risk of oxidative damage through the production of reactive oxygen species(ROS). αB-crystallin is essential in the protection of cardiac cells against ischemia-reperfusion (I/R) stresses that are enhanced by the high production of ROS [18]. Hearts that over-expressed αB-crystallin experienced less tissue damage and preserved contractile function when subjescted to *ex vivo* I/R stresses [109]. Similarly, the myocardiums of αB-crystallin-

HspB2 double knockout mice were more vulnerable to I/R stresses compared to those of wild-type mice [95]. There are at least 4 mutations in the αB-crystallin gene that lead to cardiomyopathy: R120G, D109H, R157H and G154S (1.3) [64, 116, 110].

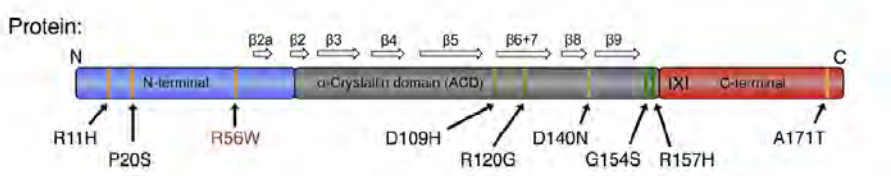

Figure 1.3: The different mutation sites on αB-crystallins. The solid black arrows show the amino acid positions at which the mutations occur. The vertical bars illustrate the phenotypes: the green bars indicate myopathy, the orange bars depict cataract and a combination of green and orange implies both cataract and myopathy. The open arrows show the different beta strands on the α-crystallin domain. Image adapted from Ref. [32]

.

The R120G mutation results in decreased chaperone activity of αB-crystallin which may prevent desmin, a substrate of αB-crystallin, to achieve and preserve its optimum folded state [20, 102]. This results in the agglomeration of desmin in inclusion bodies, leading to the weakening of cardiac muscles [18]. Aggregates formed from the αB-crystallin R120G mutants adversely affect apoptotic pathways by triggering mitochondrial dysfunction [89].

αB-crystallin is also significantly expressed in the brain and atypical amounts of cerebral αB-crystallin have been linked to neurodegenerative disorders. αB-crystallin has the highest level of expression in the brain relative to other cerebral SHSPs [77]. αB-crystallin serves a protective function under stress conditions as indicated by the increased expression of αB-crystallin under heat shock [18]. The greatest abundance of αB-crystallin in myelin sheaths further emphasizes its cerebro-protective role [118, 106]. The phosphorylated state of αB-crystallin is also influence the localization of αB-crystallin in the brain and will be further discussed in 1.1.3. αB-crystallin is also upregulated in neurodegenerative diseases such as Alzheimer's disease, Alexander's disease, Amyotrophic lateral sclerosis (ALS) and Parkinson's disease [125, 41, 111, 112, 55, 124]. A common feature of such diseases

is the presence of inclusion bodies to which αB-crystallin agglomerates.

Alzheimer's disease is characterized by neurofibrillary tangles formed by the hyperphosphorylation of a microtubule-associated protein tau and amyloid-rich plaques formed from amyloid β (Aβ) aggregates [18]. The brains of Alzheimer's patients express elevated amounts of αB-crystallin which collects in the astrocytes of Aβ aggregates [16, 133]. αB-crystallin can interact with Aβ to limit fibril elongation which reduces Aβ cytotoxicity [121, 36]. Likewise,in many of the aforementioned neurodegenarative cases, the accumulation of αB-crystallin serves to protect against of the toxicity induced by the dysfunctional clustering of proteins [37, 100, 137].

More recently, the role of αB-crystallin in cancers is being thoroughly investigated. αB-crystallin is an anti-apoptotic protein that negatively regulates proapoptic proteins such as Bax and caspase-3 [135, 63]. The upregulation of αB-crystallin expression in breast and lung cancers has enabled the use of αB-crystallin as a novel oncoprotein biomarker and as a prognosis tool for cancer [132, 136, 76, 105]. In colorectal cancer, high levels of αB-crystallin could trigger the proliferation and metastasis of tumor cells [84, 123]. αB-crystallin is also associated with other cancers and more research needs to be done to understand the role of αB-crystallin in such cases [138]. New therapeutic strategies involve targeting αB-crystallin to either selectively activate apoptosis or deflect the metastasic cascade to aid patients suffering from metastatic diseases [88].

1.1.2 Oligomerization and Subunit Exchange of α-Crystallin

SHSPs assemble into a diverse set of oligomers that differ in their number of subunits, their packing symmetry, their order and dispersity [92, 49]. While many experiments have shown the ability of αB-crystallin to limit protein aggregation, the mechanism by which αB-crystallin carries this function is not well-understood due to the lack of crystallographic information on αB-crystallin [97, 48, 39]. The polydis-

perse and dynamic nature of α-crystallin makes it hard to isolate its homodimers to characterize its high resolution structure [62]. Advances in bio-analytical methodologies have allowed the structural characterization of αB-crystallin from closer angles. This section will discuss the models proposed for αB-crystallin oligomerization and sub-unit exchange based on the evidence obtained from different analytical techniques.

The polydisperse set of αB-crystallin in solution ranges from 10-mers to 40-mers with a modal value of 28-mers [5]. Magic angle spinning (MAS) NMR showed that the basic building block of the oligomers is a homodimer (1.4) [67]. The dimer consists of two β sandwich subunits from the α-crystallin domains. The dimer interface is formed when β6+7 strands from the two subunits connect in antiparallelly [68]. An interesting feature of the homodimer is its pH-dependent curvature: while at a

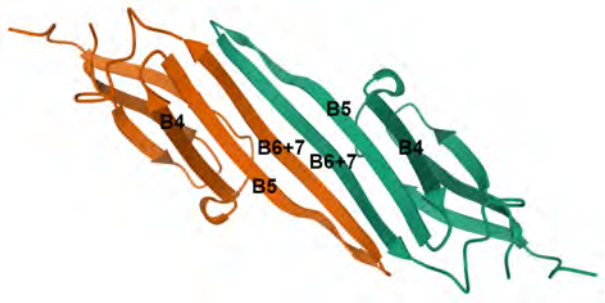

Figure 1.4: The intradimer interaction between two αB-crystallin molecules. The homodimer is formed by the antiparallel interaction between the β6+7 strands on either monomer.(PDB:2KLR)

pH of 7.5 the angle between the two β4-β5-β6+7 planes averages 121°, the angle flattens out at a pH of 9 [67]. sNMR and ssNMR studies showed that the homodimer interface is conserved in higher order oligomers [69].

A triple hybrid approach integrating cryo-EM, NMR and structural modeling traced the hierarchical assembly principle of αB-crystallin [39]. In this model, the first structural echelon is the homodimer in which the two αB-crystallin subunits differ in the orientations of their N- and C- termini with respect to their α-crystallin domains. The second sturctural level involves the interaction of three dimers to

form a hexameric subunit. The binding of the IPI motif on the C-terminus of one homodimer to the $\beta 4{+}\beta 5$ groove of the neighbouring homodimer results in the hexameric sub-unit [54]. The third structural echelon models the arrangement of hexameric substructures into 24mers via interactions of the N-terminal domains of three dimers at one of the three-fold symmetry axes on the surface [23]. The deletion of the N-terminal domain results in smaller oligomers, underlining the importance of the N-terminal domain for the formation of higher order oligomers [117]. While other models have been proposed for the formation of 24mers from αB-crystallin subunits, all agree that the arrangement of 24-mers involves a step-by-step process in which αB-crystallin monomers form homodimers that combine into hexameric sub-structures that assemble in subtly different ways to form 24-mers (1.5) [39, 24, 66, 8].

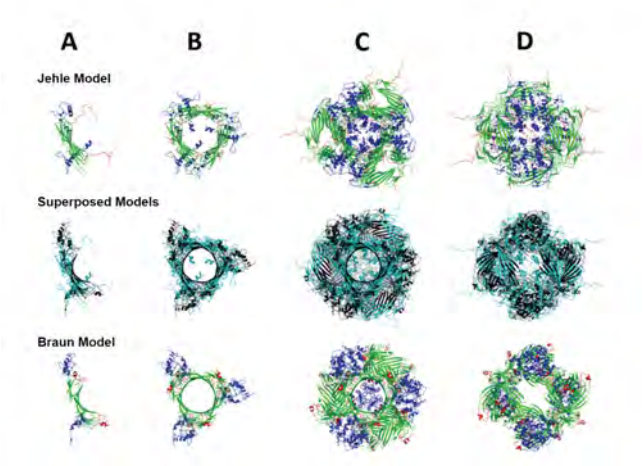

Figure 1.5: Comparison of 2 models for the structural hierarchy of αB-crystallin 24mer formation. The α-crystallin domain (green), c-terminal domain (red) and n-terminal domain (blue) are shown in different colours. The Jehle (cyan) and Braun (black) models are superposed on each others and shown in the middle row. Both models agree on the hierarchical formation of the 24mer starting from a homodimer that assembles into a hexameric subunit before arranging into higher order oligomers. The models differ in their arrangements of the N-terminal domain: the 24mer core in the Jehle model is filled with the N-terminal domain while the 24mer core in the Braun model is hollow as the N-terminal domain wraps around its surface. Adapted from Ref. [39].

In addition to existing as an ensemble of oligomeric states at equilibirum, αB-crystallin can also rapidly interconnect between these different states [58]. The rate

of subunit exchange of α-crystallin depends on several factors such as the presence of partially unfolded substrates, cellular temperature and post-translational modifications [13, 21, 103]. Studies suggest that subunit exchange is vital for the chaperone function of α-crystallins [82].

1.1.3 Phosphorylation of Alpha-B Crystallin

Phosphorylation is one of the major post-translational modifications that αB-crystallin undergoes [103]. The major phosphorylation sites of αB-crystallin are the serine residues S19, S45 and S59 found on the N-terminal domain of αB-crystallin (1.6) [7].

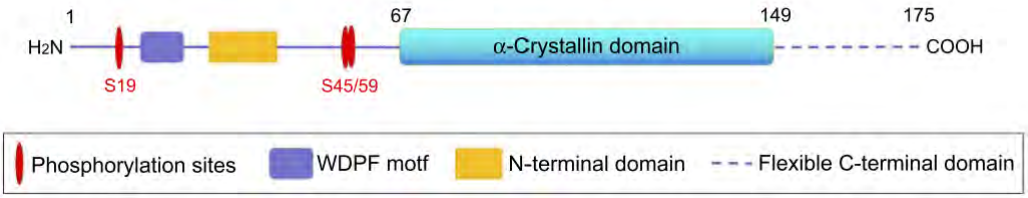

Figure 1.6: Serine residues S19, S45 and S59 on the N-terminal domain of αB-crystallin. Adapted from Ref.[[138]]

αB-crystallin and its phosphorylation are upregulated under stress conditions [119]. The phosphorylation of S59 is mediated by the MAPKAP kinase-2 pathway while S45 gets phosphorylated via p44/42 MAP kinase pathway. The pathway that phosphorylates S19 is yet unknown [6].

The phosphorylation of the N-terminal domain of αB-crystallin not only endows the domain with structural flexibility, but also helps regulate the oligomer size and chaperone activity of αB-crystallin [7, 13]. CRYO-EM studies show that phosphorylated αB-crystallin tends to form smaller oligomers such as 12mers and 6mers [13]. This is not surprising given that the phosphorylated serines tend to be negatively charged, thus repeling other phosphorylated serines and preventing them from making close contact with the phosphorylated N-terminal domain.

The effect of phosphorylation on αB-crystallin activity is still debated: while some believe that phosphorylation enhances αB-crystallin activity by increasing binding affinity for substrates, others believe that the smaller oligomer size attenuates the chaperone activity of phosphorylated αB-crystallin [2, 42, 31].

1.1.4 Research Questions

This project aims to study the pH modulation of a hyper-phosphorylated version of αB-crystallin in which the 3 serine residues S19, S45 and S59 are phosphorylated. To study the hyper-phosphorylated αB-crystallin, we will use a mutant αB-crystallin, 3E-αB-crystallin, in which the 3 serine residues have been replaced by glutamate residues to mimic the charges on the phosphorylated serines.

Light scattering assays, using insulin as an aggregation model will be used to evaluate the chaperone efficiencies of αB-crystallin and 3E-αB-crystallin under different pH environments. Single molecule Förster Resonance Energy Transfer(sm-FRET) studies will be used to probe the subunit exchange in αB-crystallin at different pH environments. Fluorescence Correlation Spectroscopy and dual-color Fluorescence Cross-Correlation Spectroscopy will be used to calculate the oligomer size and the extent of heteroligomerization between αB-crystallin and 3E-αB-crystallin.

1.2 Fluorescence

Fluorescing light bulbs, glow-sticks and light-emitting diodes(LED) are all examples of applications of luminescence, an umbrella term used to describe the emission of light by samples via non-thermal processes.Photoluminescence refers to the emission of light as a result of photon absorption. It encompasses fluorescence and phosphorescence. Thus, both fluorescence and phosphorescence involve the emission of light from a sample as a result of electronically excited states.

Visualising cells, proteins and other molecular components is key to understand the mechanisms behind biological phenomena. A better grasp of how cells and their biochemical elements work is essential to unlock efficient treatment for diseases. However, such cellular and molecular specimen are too small to be seen with the naked eyes. While microscopes have extended our ability to visualize cells, the use of fluorescence has enlarged the pool of cellular and molecular details we can see. Indeed, attaching a fluorescent probe to a specific amino acid on a residue helps localize that protein and helps track the protein's path in a cell for instance.

Phosphorescence and fluorescence differ in the lifetimes of their excited states: excited states tend to last seconds to minutes in phosphorescence while fluorescent samples tend to stay in their excited states for a period between nanoseconds and microseconds[134]. Fluorescence involves relaxation from a singlet excited state whereas phosphorescence involves relaxation from a triplet excited state[81].

The ground electron and excited electron of the molecule in the singlet excited state have opposite spins and the relaxation of the excited electron is thus allowed. In the triplet excited state however, both the ground and excited electrons have the same spins, hence resulting in a "prohibited" relaxation of the excited electron. It is thus more likely and quicker for the singlet excited state to relax to the ground state, as is the case for fluorescence.

Fluorescence, especially fluorescence microscopy, is increasingly being used to probe biological systems. Indeed, techniques such as FRET(Förster Resonance Energy Transfer), FCS(Fluorescence Correlation Spectroscopy), FRAP(Fluorescence Recovery After Photobleaching), FISH(Fluorescence In Situ Hybridization) are now established tools for the structural and dynamical studies of biological systems. This section will describe basic fluorescence lexicon while sections 1.3 and 1.4 will cover FRET and FCS, the two main techniques used in this theses, in more detail. This section has been written by drawing information from Ref. [81].

1.2.1 Fluorescence Absorption and Emission Spectra

Fluorescence is a result of transitions between quantized energy levels of fluorescent molecules (fluorophores). A Jablonski diagram depicts the transitions occuring during processes such as fluorescence and phosphorescence(1.7). In the Jablonski diagram of (1.7), the singlet ground,first and second electronic states are depicted by S_0, S_1 and S_2 respectively. The vibrational energy levels of each of the electronic states are labelled 0,1,2, inter alia.

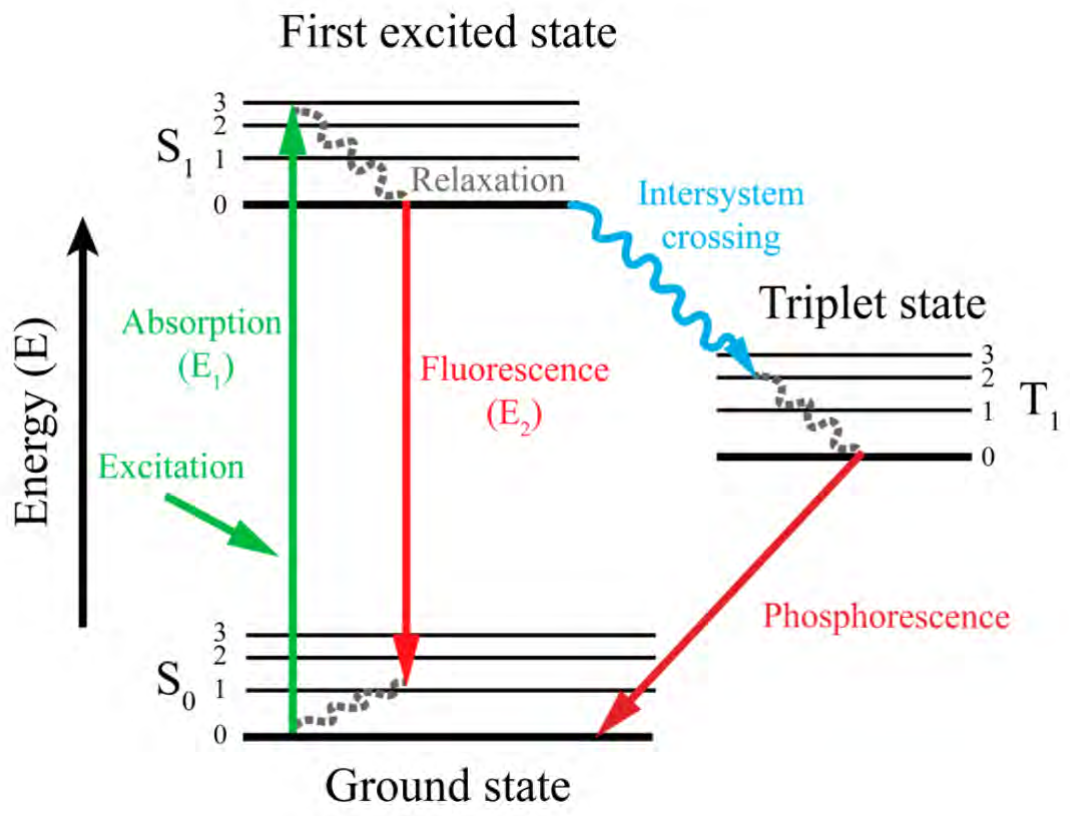

Figure 1.7: When light excites a fluorophore, the absorbed photon of energy E_1 excites the fluorophore from its ground state (S_0) to its excited singlet state (S_1). When the fluorophore fluoresces, it emits a photon of energy E_2 as it relaxes from the lowest vibrational state of S_1 to S_0. Figure adapted from Ref. [93]

At room temperature, fluorophores mainly populate the S_0 state and predominantly its lowest vibrational level. As a fluorophore absorbs a photon, it gets promoted to its first excited electronic singlet state, S_1. This transition takes place in about 10^{-15} seconds. The fluorophore in the S_1 state resides in some higher vibrational level of the S_1. The excited fluorophore undergoes internal conversion as

it rapidly relaxes to the lowest vibrational level of S_1. This relaxation occurs as the internal conversion happens within 10^{-12} seconds [81], which is much smaller than typical fluorescence lifetimes of 10^{-8}. Hence, fluorescence emission occurs from the lowest vibrational energy level of S_1. When the fluorophore relaxes from this excited state to the S_0 state via the emission of a photon, fluorescence occurs. The fluorophore usually returns to a higher excited vibrational ground state level which quickly reaches thermal equilibrium.

The transitions involved in fluorescence are described as vertical transitions as they obey the Franck-Condon principle. According to the Franck-Condon principle, when fluorophores are excited, electronic transitions happen faster than nuclei responses due to the lighter mass of electrons relative to nuclei masses. Electron density thus rapidly builds up in other parts of the fluorophore. As a result, the intially stationary nuclei start vibrating about their original positions as they are under the influence of a new force field. The original positions of the ground state nuclei thus become their turning points in their excited states.

A fluorophore can be characterized through its fluorescence spectrum. Most fluorescence spectra are represented by the fluorophore's emission spectra. The absorption spectrum shows the wavelength dependence of the light absorbed by the fluorophore while the emission spectrum illustrates the wavelength dependence of the excited fluorophore as it relaxes.

Absorption and fluorescence speactra tend to be broad because the fluorophore can relax and be excited in various ways as a result of the fluorophore's many different excited states. The energy of emission of a fluorophore is typically less than its absorption energy. This phenomenon is termed the Stoke's shift. A common cause behind the Stoke's shift is the rapid relaxation of the fluorophore to the lowest vibrational level of S_1. Another cause is the decay of most fluorophores to higher vibrational states of the ground state as this leads to further excitation energy loss by the thermalization of the excess vibrational energy. Solvent relaxation also

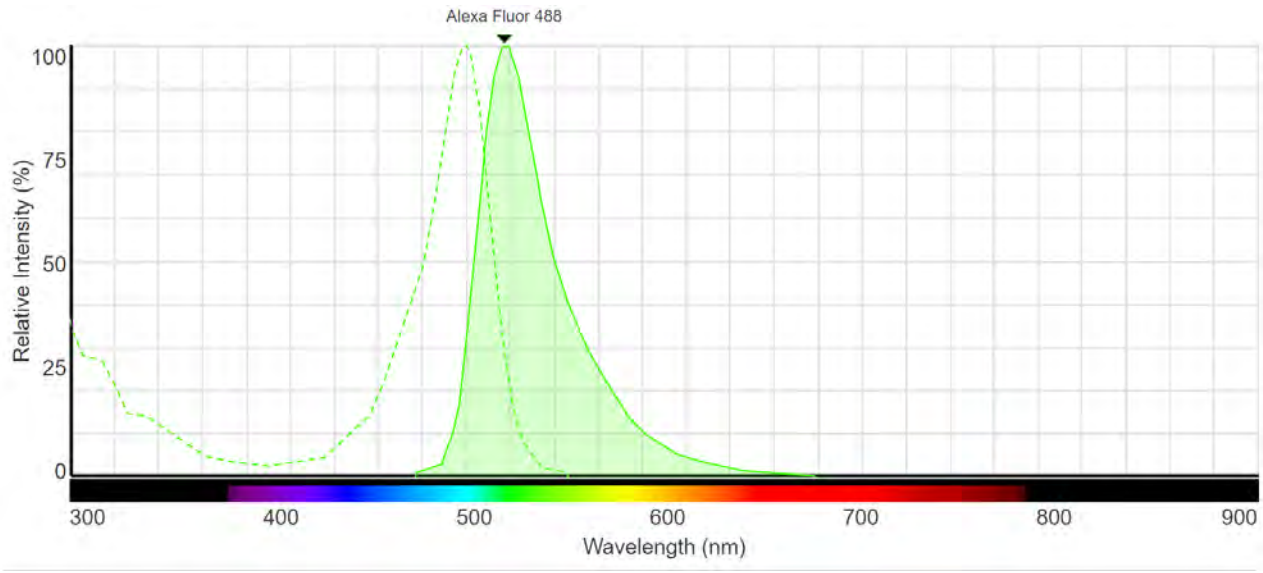

Figure 1.8: The excitation (dotted line) and emission (solid line) spectra of Alexa Fluor 488 dye produced by ThermoFisher Scientific.

contributes to Stoke's shift. Indeed, while fluorophores tend to have larger excited state dipole moments relative to their ground state, tiny solvent molecules rotate rapidly. The relatively long fluorescence lifetimes(nanoseconds) compared to solvent rotational motion(picoseconds) enables solvent molecules to re-position themselves around the excited-state dipole, thus lowering its energy. This shifts the emission to longer wavelengths. Other causes of Stoke's shift include excited-state reactions, complex formation and energy transfer. Fluorescence thus usually occurs at longer wavelengths compared to absorption wavelengths.

1.2.2 Fluorescence Quantum Yields and Lifetimes

A fluorophore tends to have distinct lifetimes and quantum yields. A fluorophore's lifetime gives an indication of the time available for the excited fluorophore to interact with its environment. The lifetime of the fluorophore refers to the average time the molecule spends in the excited state.

The quantum yield of the fluorophore refers to the number of photons emitted relative to number of photons absorbed. The quantum yield can be expressed by

the following :

$$Q = \frac{number of photons emitted}{number of photons absorbed} = \frac{\Gamma}{\Gamma + k_{nr}}, \tag{1.1}$$

where Q is the fluorophore's quantum yield, Γ is the fluorescence rate constant of the fluorophore and k_{nr} is the rate constant for non-radiative decay. Fluorophores have quantum yields that are less than one because of energy losses through Stoke's shift and quenching processes. The brightness of a fluorophore is proportional to its quantum yield.

1.2.3 Non-Emissive Electronic Relaxation Processes

There are processes other than fluorescence through which an excited molecule can relax. Quenching refers to the decrease of fluorescence intensity by other competing processes. Studying the quenching of a fluorophore gives an insight into dynamic processes in solution or in macromolecules. There are different types of quenching and this section will explore the forms of quenching most relevant to this thesis.

In collisional quenching, the excited fluorophore relaxes by the non-radiative transfer of energy to another molecule called a quencher. Collisional quenching, also called dynamic quenching, results from collisional interactions between fluorophores and quencher molecules. Examples of collisional quenchers include oxygen and electron-deficient molecules.

Static quenching involves the complex formation between a ground state fluorophore molecule and a quencher molecule. The complex formed is usually non-fluorescent and this contributes to the decrease in overall fluorescence intensity of the fluorophore. Concentration quenching is a self-quenching process in which the fluorescence intensity decreases as the fluorophore concentration increases.

1.3 Förster Resonance Energy Transfer (FRET)

Förster Resonance Energy Transfer (FRET) is one of the techniques used to study the biological system of interest in this thesis. FRET is a subset of Resonance Energy Transfer(RET) which is an example of a fluorescence quenching process.

RET involves the transfer of electronic energy from an excited molecule, the donor, to an acceptor molecule. This transfer of electronic energy helps the donor molecule relax to its ground state. The transfer is facilitated by dipole-dipole couplings between the molecules involved.

In FRET, when a donor fluorophore is excited, it can also relax by energy transfer to an acceptor fluorophore present in the reaction environment. The overall fluorescence intensity of the donor fluorophore is thus quenched as some of the donor fluorophores relax by FRET. The energy transferred to the acceptor fluorophore is enough to excite it. The acceptor relaxes by fluorescence emission, resulting in an increased overall fluorescence intensity of the acceptor molecule.

It is useful to note that FRET is a subset of RET, i.e, there are other RET processes that do not necessarily involve fluorescence emission from the acceptor molecule. An example is the RET that happens during photosynthesis. The energy from chlorophyll b, the donor, is transferred to reaction centers via chlorophyll a, the acceptor. The energy transferred is then used to initiate electron transfer reactions during photosynthesis [120].

1.3.1 Qualitative Description of FRET

FRET can be understood by thinking of the donor and acceptor fluorophores as dipoles. On top of emitting a photon of lower energy via fluorescence, the donor fluorophore dipole also starts to oscillate, thus generating an electric field. As the acceptor fluorophore dipole feels the oscillating electric field, it absorbs the energy

at a resonant frequency. Since the acceptor is now excited, it fluoresces to relax. The overall FRET event is characterized by a decrease in the fluorescence intensity of the donor and an increase in the fluorescence intensity of the acceptor.

1.3.2 Criteria for FRET

Förster, who helped improve the theoretical treatment of RET, underlined that there were two main features on which energy transfer depended [70]. The first factor is spectral overlap of the donor and acceptor pair. Indeed, the donor emission spectrum should overlap to a certain degree with the acceptor excitation because the energy emitted by the donor has to be enough to excite the acceptor for FRET to take place. It is needless to say that in an ideal donor-acceptor pair, the donor excitation should have no direct influence on the acceptor excitation and thus acceptor emission. This ensures that any acceptor molecule excitation and emission solely comes from the energy transfer from the donor molecule. The second factor is the distance between the donor-acceptor pair.

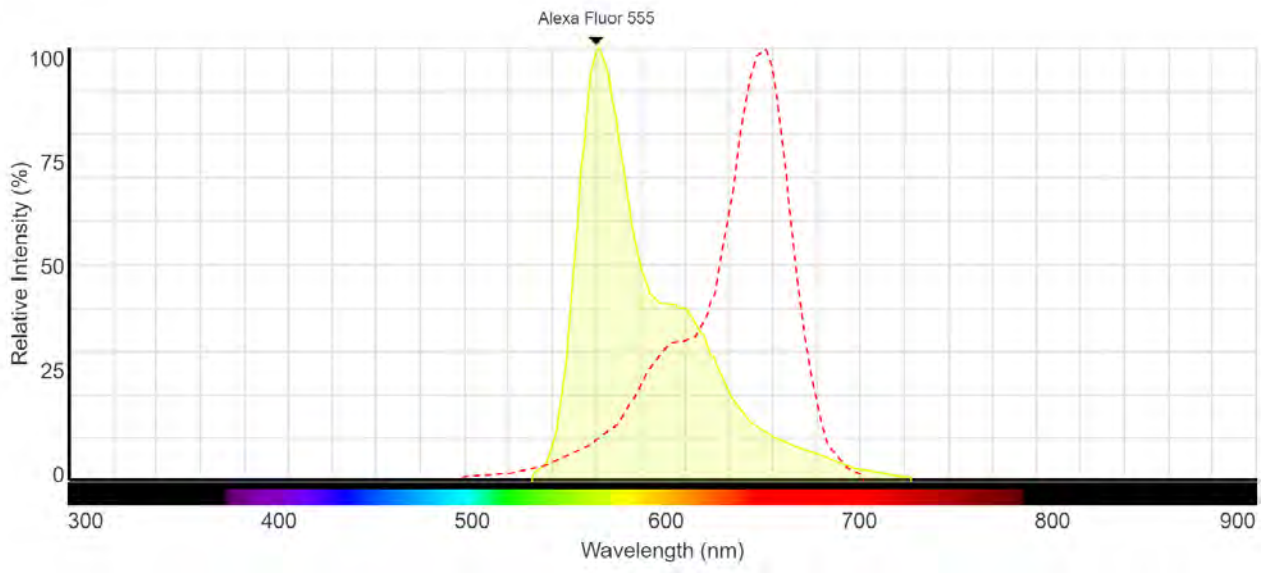

Figure 1.9: The emission spectrum (solid green) of Alexa Fluor 555 greatly overlaps with the excitation spectrum (dotted red) of Alexa Fluor 647. Here, the donor dye is Alexa Fluor 555 and the acceptor dye is Alexa Fluor 647.

1.9 shows the spectral overlap between Alexa Fluor 555 and Alexa Fluor 647.

1.3.3 Measuring FRET

Experimentally, FRET in a system is gauged through the FRET efficiency as it represents the extent to which FRET happens. The dependence of FRET efficiency on small-scale distances(10 to 100 Å) is given by the following equation:

$$E = \frac{{R_0}^6}{{R_0}^6 + r^6}, \tag{1.2}$$

where R_0 is the Foïrster distance and r is the intermolecular distance between the donor and acceptor. R_0 is the intermolecular distance at which half of the energy is transferred. Equation 1.2 can be reached by treating FRET either classically or via quantum mechanics. During FRET, the acceptor molecule gets excited by the donor molecule without any photon re-emission by the donor molecule. It is only the energy of the donor that gets transferred to the acceptor via resonance. Experimentally, FRET efficiency is measured as follows:

$$E = 1 - \frac{F_{DA}}{F_D}, \tag{1.3}$$

where F_{DA} is the fluorescence intensity of the donor in the presence of the acceptor and F_D is the fluorescence intensity of the donor only. The FRET efficiency obtained in this way is then used to calculate the distance between the acceptor and donor fluorophores using Equation 1.2.

1.3.4 Single Molecule FRET

Single molecule techniques enable us to manipulate and study individual molecules, enabling us to view biological systems from a new angle. Single molecule FRET (sm-FRET), was first performed in 1996 and has since become one of the most general

single-molecule techniques [115]. smFRET has unlocked some of the many secrets of folded proteins, motor proteins and non-canonical DNA dynamics [115]. More details about the apparatus used for smFRET are given in Section 2.

1.4 Fluorescence Correlation Spectroscopy(FCS)

Fluorescence Correlation Spectroscopy (FCS), is another technique used in this project to probe our system of interest. FCS was simultaneously developed by Rudolf Rigler from the Karolinska Institute and Elliot Elson from Cornell University in the early 1970s [44]. Their idea was to follow kinetic processes through analysis of equilibrium fluctuations by observing the fluorescence changes in the system under study [114]. The incorporation of confocal microscopy to FCS has helped increased its sensitivity and has brought FCS to the biophysical forefront [130]. Today, FCS is an established method being used to study enzyme kinetics, molecular transport, protease activity, binding activities and to elucidate membrane structure.

1.4.1 Description of FCS

In FCS, fluorescence is recorded as fluorophore-tagged molecules pass through an illuminated observation volume, as shown in 1.10. As fluorophores pass through the illuminated volume, they get excited and fluoresce. The fluorescence intensity fluctuates as the fluorophores move in and out of the illuminated volume. The fluorescence fluctuation is analysed to extract dynamic information such as the diffusion coeficient of the molecules.

FCS depends on the spontaneous fluctuations of fluorescence intensity caused by deviations from a mean. An important parameter in FCS is the autocorrelation function. Autocorrelation reflects the degree of similitude in a time signal. In the case of FCS, $F(t)$, the fluorescence signal at a certain time, is measured against the

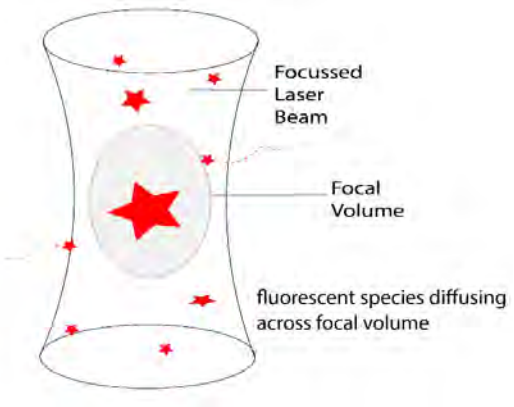

Figure 1.10: In a typical FCS setup, excitation is accomplished with a laser that is focused to a diffraction-limited spot. The illuminated observation volume is defined by its Gaussian characteristic.

time-averaged signal, $< F(t) >$. The time-dependent fluctuation is then given by:

$$\delta F(t) = F(t) - < F(t) > . \tag{1.4}$$

The intensity information in FCS is preserved because the autocorrelation is calculated from the time trajectories of the fluorescent signal. When a confocal set-up is used, the fluctuations from the time average result in an autocorrelation curve which is defined by:

$$G(\tau) = \frac{< \delta F(t)\delta F(t+\tau) >}{< F(t) >^2}. \tag{1.5}$$

The autocorrelation $G(t)$ is calculated with respect to the self-similitude of the fluorophore moving in and out of the observation volume after lag time (τ) under laser irradiation. Fitting a mathematical model to the autocorrelation curve then provides information such as diffusion coefficients (D), diffusion time (τ_D), number of molecules in the observation volume ($< N >$) and molecular brightness (η). In free solution measurements, the observation volume is modeled by characterized by a 3D Gaussian profile. This enables the use of a 3D Brownian diffusion model to

express the autocorrelation function as follows:

$$G(\tau) = \frac{1}{< N >}(1 + \frac{\tau}{\tau_D})^{-1}(1 + \frac{\tau}{\tau_D S^2})^{-1/2}. \tag{1.6}$$

The 3D diffusion model enables the extraction of useful dynamic parameters from the autocorrelation function. The term S represents the shape of the observation volume and is given by ratio of the z and xy radii of the volume. The diffusion coefficient obtained can then be used to find the mass of the molecule under study as shown in Section 2. The qualitative description of FCS in this section were primarily inspired from Ref. [130].

1.4.2 Fluorescence Cross-Correlation Spectroscopy(FCSS)

A major drawback of FCS is its inability do detect bound and unbound species and complexes. In enzyme kinetics for instance, the change in mass between the enzyme and enzyme-substrate complex is typically too small to be recognized by FCS. Fluorescence Cross-Correlation Spectroscopy (FCCS) was developed to solve this limitation.

In FCCS, the molecules under study are labeled with two different fluorophores that are excited by two different lasers. The fluorescence signal collected is divided into two different channels. The two fluorescence signals (e.g red and green) are measured simultaneously and cross-correlated. Only bound molecules that contain the different fluorophores are cross-correlated. FCCS requires that the fluorophores chosen have very different emission peaks to avoid cross-talk. The details about the FCS and FCCS experiments set-up will be further discussed in Section 2.

Chapter 2

Materials and Methods

2.1 Experimental Design

The main goal of this project was to compare the functional and dynamical characteristics, in different pH environments, of αB-crystallin and its hyperphosphorylated version using the phosphorylation mimic, 3E-αB-crystallin as proxy. Fluorescence Correlation Spectroscopy (FCS) was chosen to gain insight about the oligomeric states of the species at different pH environments due to its ability to report size information. Likewise, Fluorescence Cross-Correlation Spectroscopy (FCCS) would indicate the extent hetero-oligomers and homo-oligomers in the pH media. The single molecule Förster Resonance Energy Transfer (smFRET) experiments would provide us with insight about the dynamics of sub-unit exchange in our systems. The chaperone aggregation assays would probe how efficient our α-B-crystallin and the 3E-αB-crystallin are under different pH conditions.

We decided to evaluate the dynamics and performance of our system *in vivo* at the physiological pH of 7.4. We also investigated the behaviour of αB-crystallin at the pH to 6.5 to mimic the slightly acidic environment that develops in the eye lens as we age. We also studied our system at the basic pH of 8.3.

This section is intended to be a comprehensive guide to the reader who wishes to reproduce similar studies.

2.2 Preparation of Experimental System Components

2.2.1 Fluorescent Labeling

Dye Selection

Invitrogen Alexa Fluor Dyes were obtained from Molecular Probes(ThermoFisher Scientific). The fluorescent probes chosen were succinimidyl (NHS) esters that are amine-reactive. The labeling of the proteins was carried out at a pH of 8.3 to favor the conjugation of the dye probes to lysine residues on the proteins.

Invitrogen Alexa Fluor 488 (NHS ester) and Invitrogen Alexa Fluor 647 (NHS ester) were chosen for the FCS and dual-color FCCS experiments. The two dyes were chosen for the minimal spectral cross-talk between them, as shown in 2.1.

Invitrogen Alexa Fluor 555 (NHS ester) and Invitrogen Alexa Fluor 647 (NHS ester) were chosen as donors and acceptors respectively for the smFRET experiments as explained in Section 1.

Protein Labeling

The following describes the protocol followed to label the wild-type αB-crystallin and 3E-αB-crystallin with the dyes Invitrogen Alexa Fluor 488(NHS ester), Invitrogen Alexa Fluor 555(NHS ester) and Invitrogen Alexa Fluor 647(NHS ester). The general protocol for any of the three types of dye will be summarized below.

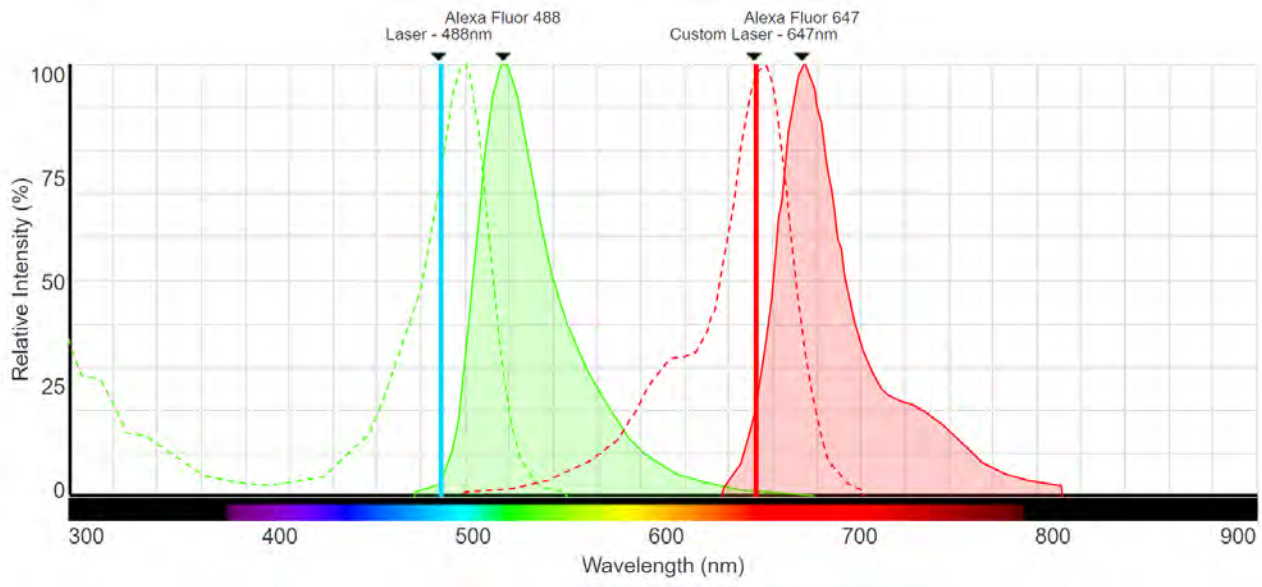

Figure 2.1: There is little spectral overlap between the emission and excitation spectra of Invitrogen Alexa Fluor 488 and Invitrogen Alexa Fluor 647. The excitation spectrum (dotted green) of Alexa Fluor 488 and its emission spectrum (solid green) are shown. The excitation spectrum (dotted red) of Alexa Fluor 647 and its emission spectrum (solid red) are also shown. The excitation laser wavelengths of 488 nm (solid blue) and 647 nm (solid red) are also included. Adapted from Ref.[4]

The labeling reactions are carried out at a pH 8.3 to promote the conjugation of the dye probes at the lysine residues. The labeling reactions were carried out in 0.1 M sodium bicarbonate buffer at pH 8.3. The different protein samples were all buffer exchanged into the 0.1M sodium bicarbonate buffer (pH 8.3) as explained in 2.3.1.

The labeling reaction was carried out in an Eppendorf tube wrapped with aluminium foil to minimize exporsure to light . 80 μL of 0.1 M TRIS-HCl (pH 7.4) was added to 120 μL of 40 μM of α-crytallin in 0.1 M sodium bicarbonate buffer (pH 8.3). The TRIS-HCl was added to react with the free NHS dye left in the reaction mixture due to the presence of an amine group on TRIS (tris(hydroxyethyl)aminomethane). The dye stock from 2.2.2 was diluted to 400 μM with Molecular Probes Anhydrous DMSO. 5 μL of 400 μM NHS ester dye was added to the TRIS-HCl / α-crystallin mixture. The reaction was allowed to proceed at room temperature for 1 hour. The following section explains how free dye was removed from the Alexa Fluor-α-crystallin conjugate mixture.

Dye Removal Protocol

After the dye and α-crystallin were allowed to react for one hour, the reaction mixture was passed through a GE Healthcare PD SpinTrap G-25 column that was first equilibrated with 0.1 M sodium bicarbonate buffer (pH 8.3). The column was spun at 2500 rpm for one minute. The filtrate collected was passed through another GE Healthcare PD SpinTrap G-25 column and spun in a similar way.

3 μL of 2M Guanidine-HCl was added to the final filtrate collected to unfold the α-crystallin sample involved. This was an endeavor to liberate any free dye molecules either loosely bound by non-covalent bonds to residues on the α-crystallin sample or trapped in folds of α-crystallin. The mixture of Guanidine-HCl and Alexa Fluor-α-crystallin conjugates was allowed to react for 3 hours at room temperature.

The mixture of Guanidine-HCl and Alexa Fluor-α-crystallin conjugates was then transferred to Thermo SCIENTIFIC Slide-A-Lyzer MINI Dialysis Units (MWCO: 20000). The dialysis units were placed in floaties and left in a refolding buffer(see section 2.2.2) for 12 hours at room temperature. The dialysis buffer (in this case the refolding buffer) was replaced with a fresh sample of buffer once throughout the duration of dialysis.

Buffer exchange was performed to transfer the Alexa Fluor - α-crystallin conjugate from the refolding buffer to a final buffer of the desired pH at which the α-crystallin sample would be studied. The Alexa Fluor - α-crystallin conjugate was again transferred to Thermo SCIENTIFIC Slide-A-Lyzer MINI Dialysis Units (MWCO: 20000). In this case, the dialysis units were placed in the final buffer of a desired pH for 12 hours at room temperature. The dialysis buffer (in this case the final buffer of a desired pH) was also replaced once by a fresh sample of buffer throughout the dialysis period.

Dye Removal Characterization

The concentration of Alexa Fluor (NHS ester) fluorophore present at each step of the purification was monitored through absorbance spectra taken at every step of the free dye removal process using the DeNovix DS-11 Spectrophotometer, as shown in Fig. 2.2.

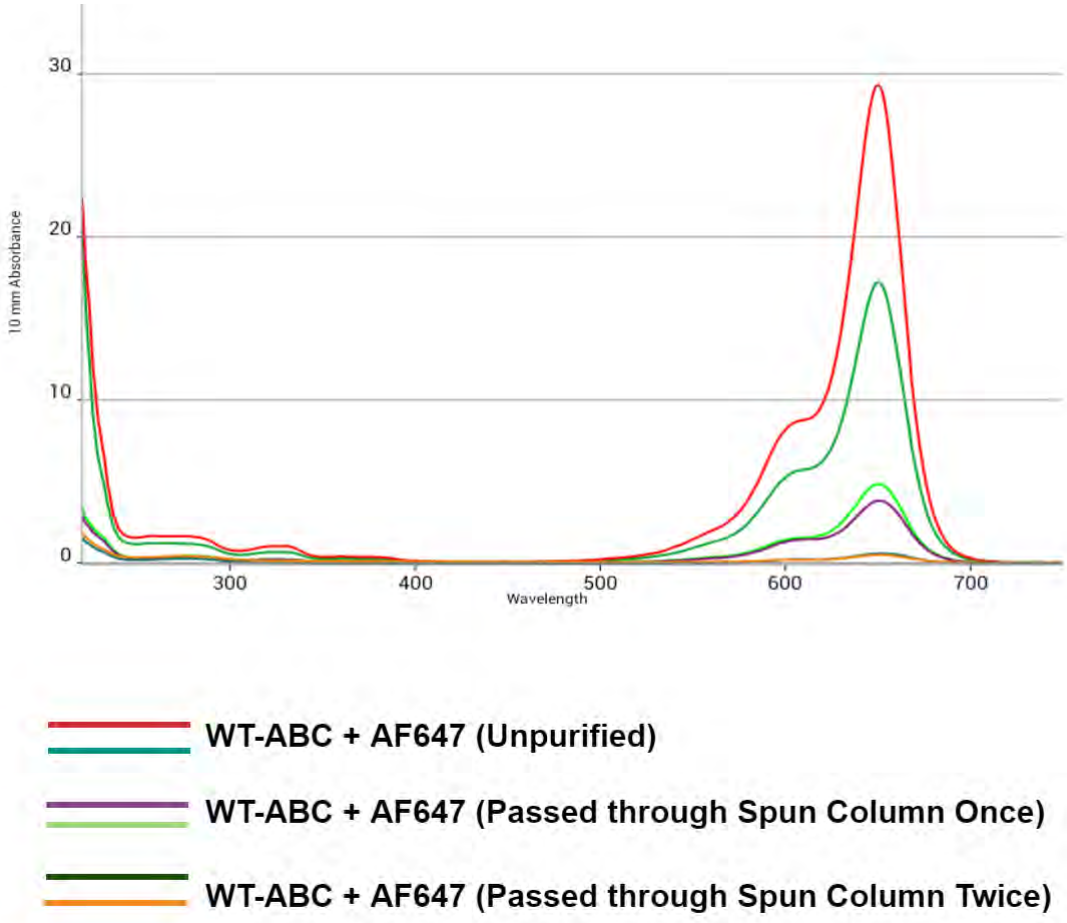

Figure 2.2: Wild type αB-crystallin (WT-ABC) was reacted with Alexa Fluor 647 NHS ester (AF647). The absorbance spectra shown here show the gradual reduction in absorbance at around 650 nm as the WT-ABC/AF647 samples are passed through GE Healthcare PD SpinTrap G-25 spun columns twice.

Since it was essential to get rid of most of the free dye left in the αB-crytallin/Alexa Fluor NHS ester reaction sample for limitedly skewed FCS and smFRET experiments, we decided to use visible fluorescence gel imaging to probe whether our system still contained a considerable concentration of free Alexa Fluor molecules

that did not not bind to lysines.

An SDS-PAGE was first carried out using the protocol established in the Jaswal laboratory. The SDS-PAGE enabled our samples to denature and liberated any free dye molecule that could have been stuck in a protein ridge or that could have been loosely (non-covalently) bound to the protein. The dye molecules, being much lighter than our αB-crystallin (20kDa), were expected to travel much faster and were expected to collect at the bottom of the gel. Once the SDS-PAGE had finished running, the Azure 600 Imaging System from the Bishop laboratory was used to characterize any fluorescence present in the unstained gel, as shown in Fig. 2.3.

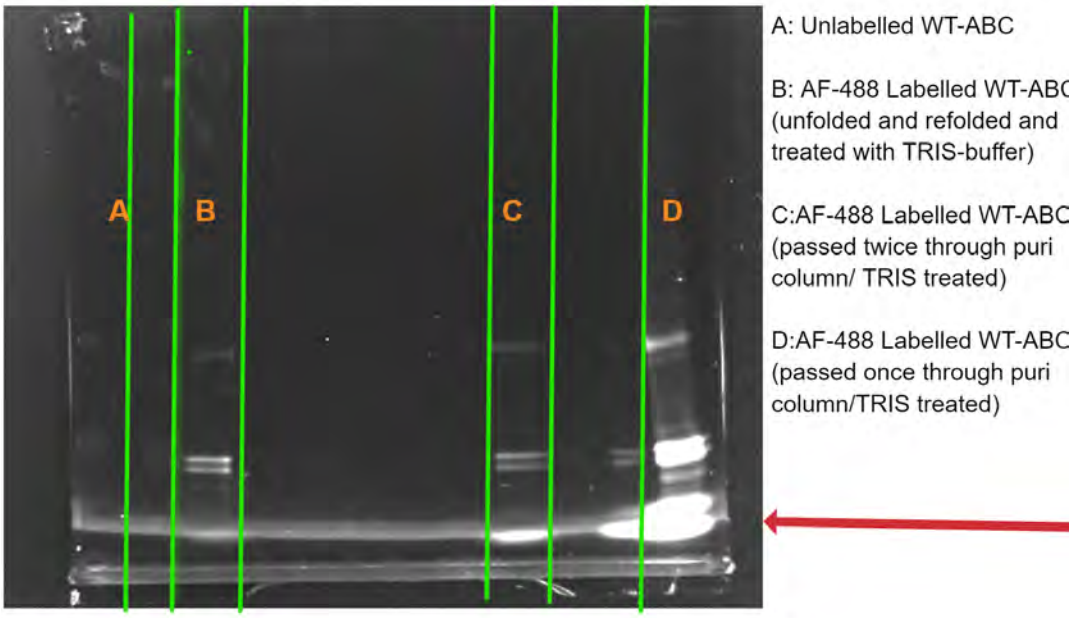

Figure 2.3: An SDS-PAGE of the differnt levels of purification of the mixture of wild-type αB-crystallin (WT-ABC) and Alexa Fluor 488 NHS ester (AF488) was performed. The gradual decrease in brightness of fluorescence at the bottom of each lane indicated the decreasing concentrations of free Alexa Fluor 488 dye molecules present at different steps of the purification.

The fluorescence imaging system is not sensitive below a certain free dye concentration present in our system. However, FCS experiments allowed us to identify the presence of free dye molecules in our system.

2.2.2 Stocks and Recipes

α-Crystallin Stocks

The wild type αB-crystallin and 3E-αB-crystallin stocks were obtained from Professor James Hebda at Austin College.

The α-crystallin (from bovine eye lens) stock, which contains both αA-crystallin and αB-crystallin, was obtained as a lyophilized powder from Millipore Sigma. The α-crystallin powder was dissolved in 0.1 M sodium bicarbonate buffer at pH 8.3 and stored at -20 ℃.

Insulin Stocks

Human recombinant insulin was obtained as a lyophilized powder from Millipore Sigma. 20 mg of the insulin powder was dissolved in a minimum of 0.1 M HCl (hydrochloric acid) and was made up to 10 mL using MiliQ water to obtain an insulin stock of 2 mg/mL. This was stored at -20 ℃.

Dye Stocks

1 mg of Invitrogen Alexa Fluor NHS ester dye is dissolved in 100 μL of Molecular Probes Anhydrous DMSO. The 100 μL of dye stock is divided into 5 aliquots of 20 μL and stored at -80 ℃.

Refolding Buffer Recipe

To prepare the refolding buffer, 60 mL of 1 M sodium bicarbonate buffer (pH 8.3) was added to 180 mL of MiliQ water and 30 mL of 5 M urea and thoroughly stirred.

2.3 Chaperone Activity Assays

Chaperone activity assays were performed to probe the chaperone efficiency of wild-type αB-crystallin and 3E-αB-crystallin in Bis-TRIS (pH 6.5), TRIS-HCl (pH 7.4) and sodium bicarbonate (pH 8.3). Since αB-crystallin is a promiscuous chaperone, its ability to prevent the aggregation of denatured insulin under different pH environments was exploited to investigate its chaperone efficiency.

Insulin consists of insulin A and insulin B chains that are held together by disulfide bonds. The addition of DTT reduces the disulfide bonds, separating the insulin chains which aggregate over time. The presence of αB-crystallin limits this aggregation.

In this assay, the reduction in insulin aggregation served as a reporter of the chaperone efficiency of the αB-crystallin sample under study. Light absorbance was used as a surrogate measurement for the light scattered by the insulin aggregates. Monitoring the light absorbance thus helped track the insulin aggregation.

2.3.1 Sample Preparation

α-Crystallin Preparation

Aliquots from the α-crystallin stocks were buffer exchanged to a buffer of desired pH by first loading 100 μL of the α-crystallin on a Corning Spin-X UF 500 concentrator (MWCO 10k). 100 μL of the buffer of desired pH was also loaded on the concentrator. The concentrator was centrifuged at 6500 rpm for 10 minutes. 100 μL of the buffer at desired pH was again added and the concentrator was spun at the same speed and for the same duration. This last step was performed thrice. The newly buffer-exchanged α-crystallin sample was then collected and diluted to 40 μM with the buffer at desired pH. The α-crystallin sample was allowed to incubate at

the new pH overnight at 4 ℃.

Insulin Preparation

Aliquots from the insulin stock were buffer exchanged to a buffer of desired pH by first loading 100 μL of the insulin on a Pierce Concentrator (MWCO 3k). 100 μL of the buffer of desired pH was also loaded on the concentrator. The concentrator was centrifuged at 15000 rpm for 20 minutes. 100 μL of the buffer at desired pH was again added and the concentrator was spun at the same speed and for the same duration. This last step was performed thrice. The newly buffer-exchanged insulin sample was then collected and diluted to 40 μM with the buffer at desired pH. The insulin sample was allowed to incubate at the new pH overnight at 4 ℃.

2.3.2 Assay Set-Up

A vial of Pierce DTT, No-Weigh Format was removed 3 hours before the assay and was allowed to reach room temperature. Similarly, the α-crystallin and insulin samples were allowed to reach room temperature one hour before starting the experiment.

The experiments were run in Nunc 96-well, clear, flat-bottomed microplates. 40 μL of 40 μM insulin was added in each well. 40 μL of 40 μM αB-crystallin or 40 μL of MiliQ water for the control was added to the insulin and mixed by pipetting with care to avoid the appearance of bubbles. The Pierce DTT was dissolved in 100 μL to make up 500 mM of DTT solution. 5 μL of DTT solution was added to each insulin well under study. The assay solution was mixed carefully by pipetting. Absorbances of the uncovered wells at 340 nm and 480 nm were taken at 1 minute intervals for 3 hours using a Molecular Devices SpectraMax M5 Microplate Reader.

2.4 FCS

The FCS experiments were performed at the University of Massachusetts, Amherst, in Professor Anne Gershenson's laboratory. FCS experiments were carried out with wild-type αB-crystallin and 3E-αB-crystallin samples at pH 6.5 and pH 8.3. This section will summarize the optical set-up of the FCS apparatus, the protocol of the FCS experiments and how the FCS data were analysed.

2.4.1 The FCS Optical Apparatus

FCS is a highly sensitive technique that uses a combination of laser optics, confocal microscopy and photodiode detectors to probe systems at nanomolar concentrations. Figure 2.4 shows the general outline of the FCS system used.

The excitation source of the setup consists of a Melles-Griot air-cooled continuous wave argon-krypton 643 laser. We carried out FCS on freely diffusing αB-crystallin molecules attached to fluorescent probes. The laser beam was focused to a diffraction-limited spot to excite our sample. The confocal pinhole found inside the Olympus FluovieW confocal microscope rejects the out-of-focus light outside the observed volume. The optical parameters used ensure that observed volume is an ellipsoid that is elongated along the optical axis [81]. The average number of molecules in the observation depends on the bulk concentration and stays constant during a stationary experiment. However, the random diffusion of fluorescent molecules causes time-dependent changes that result in fluctuations in the number of fluorophores that occupy the volume. This fluctuation in the number of fluorophores occupying the observation volume results in fluctuations in fluorescence intensity. The changes in fluorescence intensity can be used to generate a cross-correlation function, as explained in the introductory chapter of this thesis.

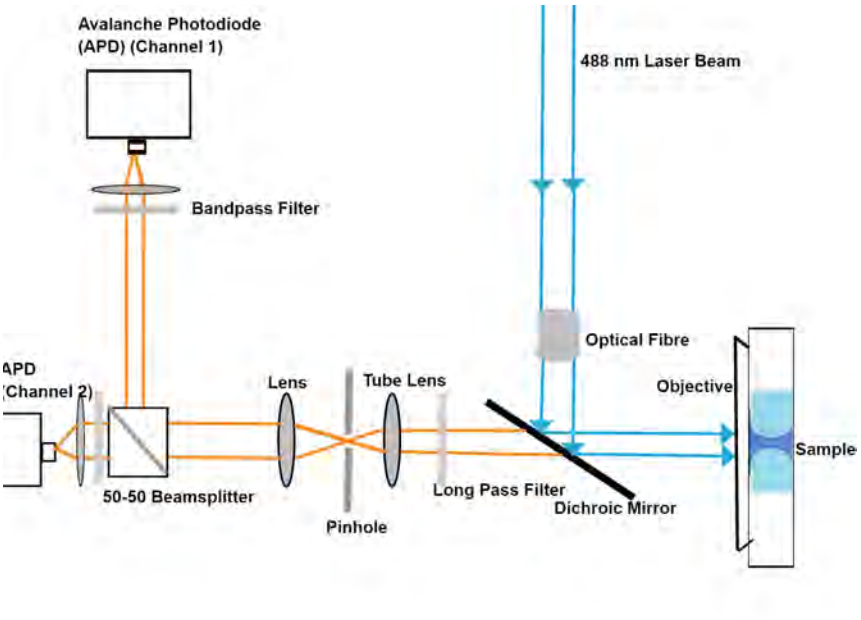

Figure 2.4: The sketch shows the main optical components that make up the FCS set-up. The scheme was made from Mind the Graph Infographic Maker and the "sample" image was obtain from Dr. Anne Gershenson.

The focused laser is assumed to have a Gaussian intensity profile, as shown in Fig 2.5. The radius ω_0 and half-length z_0 are defining features of the observation volume.

In most FCS experiments, the diffraction-limited volume usually is defined by an ω_0 of 0.25 μm and a z_0 of 1 μm, giving an effective volume of 0.35 fl. An effective volume is considered instead of the geometric volume of an ellipsoid because the observation volume does not have sharp boundaries. Fluorophore concentrations ranging from 9.6 nm to 96 nm result in 2 to 20 fluorophore molecules occupying the observation volume.

The correlation function can also be expressed as follows:

$$G(\tau) = G(\tau = 0)(1 + \frac{\tau}{\tau_D})^{-1}(1 + \frac{\tau}{\tau_D S^2})^{-\frac{1}{2}} \tag{2.1}$$

where

$$\tau_D = \frac{\omega^2}{4D} \tag{2.2}$$

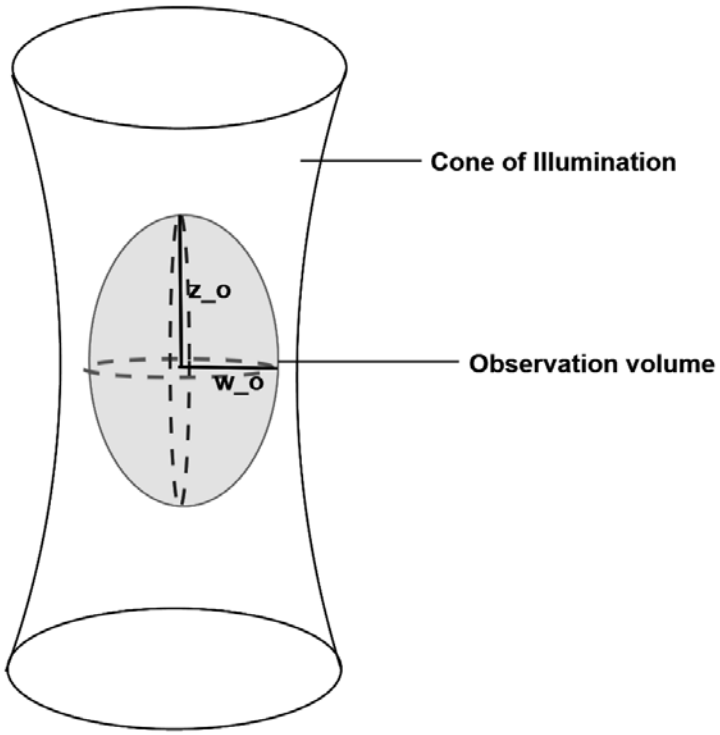

Figure 2.5: The focused laser at the observation volume has a 3D Gaussian intensity profile. Radius ω_0 and half-length z_0 refer to the distances at which the intensity decreases to e^{-2} of its maximal intensity. Image made with Adobe Illustrator.

and

$$\tau_D S^2 = \frac{{z_0}^2}{4D}. \tag{2.3}$$

It is important to know that in our experiment, we obtained values of D for the various samples through our FCS experiments to later extract size information from them. However, the recovered value of D depends on the accurate value of the effective volume. Since there are no geometric expressions that accurately describe the effective volume, FCS instruments need to be calibrated with fluorophores of known diffusion coefficients to obtain an accurate estimate of the effective volume.

2.4.2 FCS Experiments

The samples to be studied via FCS were transported with dry ice to the University of Massachusetts, Amherst. We used a laser excitation wavelength of 488nm to

study our samples which were thus labeled with Molecular Probes Alexa Fluor 488 (NHS Ester). A 647/488 nm dichroic mirror, a 30 μm pinhole and 525/50 bandpass were used in the FCS instrument (Fig . 2.4). The laser power before the optical fibre was 190 $\pm$ 1 μW. The laser power after the optical fibre was 64 $\pm$ 1 μW. A total neutral density index of 1.3 was used throughout the experiments, resulting in a laser power (after fibre) of 1.4 μW. A sampling frequency of 24 MHz was used throughout the experiments.

FCS Calibration

Rhodamine 110 from Sigma Aldrich was used to calibrate the FCS system. Starting from a stock of 10 nM, Rhodamine 110 was serially diluted to obtain sample concentrations of 7.5 nM, 5 nM, 3.75 nM and 2.5 nM. FCS experiments in which 1000000 data points were collected, were carried out for the five concentrations of Rhodamine 110 aforementioned. The serial dilutions were carried out using thrice-filtered 0.1 M TRIS-HCl at pH 7.4.

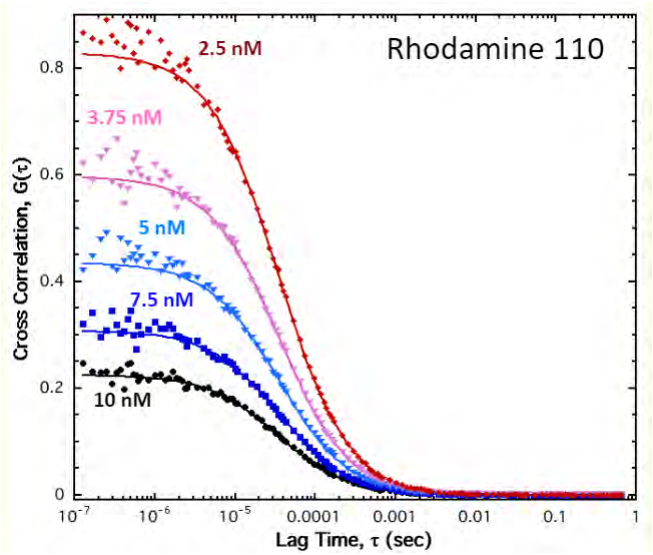

Figure 2.6: Rhodamine 110 at different concentrations were used to extract an average value for τ_D to estimate the effective volume of our FCS system.

The diffusion coefficient of Rhodamine 110 at the temerature prevalent on the ex-

periment day was known to be 470 $\mu m^2 s^{-1}$. A global correlation fit was run on all 5 FCS data obtained from the different Rhodamine 110 concentrations with the diffusion coeeficient of 470 $\mu m^2 s^{-1}$ as a fixed parameter. The global correlation fit provided us with an average of the effective volume that was defined by an ω_0 of 0.329 μm and a $\frac{z_0}{\omega_0}$ ratio of 7.53. These values of ω_0 and $\frac{z_0}{\omega_0}$ were kept as fixed parameters when determining the diffusion coefficients of our αB-crystallin samples.

FCS Experiments Protocols

FCS experiments were carried out on Alexa Fluor 488-labeled wild-type αB-crystallin and 3E-αB-crystallin at pH 6.5 and pH 8.3. All protein samples were allowed to come to room temperature before any FCS experiment was started.

The αB-crystallin samples were diluted before-hand to an estimated nanomolar concentration. The NanoDrop and UV-Vis were not sensitive enough to give an accurate value for the concentrations of αB-crystallin under study. However, that was not an issue because concentration information could be extracted from the FCS data. Since the αB-crystallin sample concentrations were already less than 5-10 nM, no serial dilution was carried.

Instead, 10 runs of 100000 were performed to obtain 1000000 data points. That allowed us to eliminate any skewed and dissimilar runs before carrying out a global correlation fitting.

In each experiment, 300 μL of the sample under study was carefully loaded on a Lab-Tek II Chamber Slide System 8-Well Glass Slide. The ISS Vista Fluorescence Correlation Spectrometer software was programmed to automatically collect 100000 data points 10 times with a 10 seconds break between each run.

2.4.3 FCS Data Analysis

FCS Evaluation Software

The FCS data obtained were analysed using the PyCorrFit Python code from Ref. [96]. All fitting models used were weighted fits. A weighted fit provides less significance to less precise measurements and more significance to more precise measurements when determining unknown parameters such as diffusion coefficients in a certain model.

The 3-D Gaussian model described so far in this thesis represents one of many models that could be used for FCS data fitting. X^2 values were used to judge how good our fitting models were. In most of the experiments, our treatment of our system using a 3D-Gaussian model turned out to be too simplistic. We instead used a 2-species diffusion model to treat some of the samples that still contained some free nhs dye molecules. In other cases, using a triplet-blinking model to cater for some of the photochemistry helped improved the X^2. More details about the models and code used are found in the Appendix section.

2.4.4 From Diffusion Coefficient to Size Information

The hydrodynamic radius, R, of our sample can be found using the following equation:

$$D = \frac{kT}{6\Pi\eta r} \tag{2.4}$$

where k is the Boltzmann's constant, T is the temperature and η is the viscosity of the solvent.

Chapter 3

Results and Discussion

Chapter 4

Conclusion

Chapter 5

Appendix